Effect of ^{11}B substitution on the superconductivity of $MgCNi_3$

T. Klimczuk,[1,2] M. Avdeev,[3,*] J. D. Jorgensen,[3] and R. J. Cava[1]
[1]*Department of Chemistry, Princeton University, Princeton, New Jersey 08544, USA*
[2]*Faculty of Applied Physics and Mathematics, Gdańsk University of Technology, Narutowicza 11/12, 80-952 Gdańsk, Poland*
[3]*Materials Science Division, Argonne National Laboratory, Argonne, Illinois 60439, USA*
(Received 18 December 2004; published 24 May 2005)

The crystal structure of boron-doped superconducting $MgC_{1-x}{}^{11}B_xNi_3$, studied by powder neutron diffraction, is reported. The solubility limit of boron is determined to be approximately $x=0.16$. The unit cell expands from $a=3.810\,89(2)$ Å to $3.819\,66(2)$ Å as x increases from $x=0$ to $x=0.155$. Boron (^{11}B) doping decreases T_c with increasing x: from 7.09 K ($x=0$) to 6.44 K ($x=0.155$).

DOI: 10.1103/PhysRevB.71.184512 PACS number(s): 74.70.Ad, 74.62.Dh

I. INTRODUCTION

The discovery of superconductivity in MgB_2 (Ref. 1) motivated a search for new superconducting materials containing light elements such as magnesium, boron, and carbon. Surprisingly, superconductivity was discovered in $MgCNi_3$ ($T_C=7$ K), in which the high proportion of Ni metal suggests that magnetic interactions may result in ferromagnetism rather than superconductivity.[2] Band-structure calculations show a narrow peak in the vicinity of the Fermi energy (E_F).[3–9] However, the density of states (DOS) at E_F is not believed to be big enough to yield ferromagnetism.[6] The presence of the DOS peak, although with lower intensity, was confirmed by photoemission and x-ray spectroscopy experiments.[7,10]

Shim *et al.* showed that the Fermi surface is composed of two bands and proposed that the strong, narrow DOS peak, located just below E_F, corresponds to the π^* antibonding state of Ni 3*d* and C 2*p*, but with a predominant Ni 3*d* character.[6] Therefore, hole doping of $MgCNi_3$ in attempts to move the Fermi level into the DOS peak should be of interest. However, neither increasing T_C nor ferromagnetism was observed with the partial substitution of Co, Fe, Ru, or Mn for Ni (Refs. 11–15) or with inducing carbon deficiency.[16,17]

The carbon atom in $MgCNi_3$ plays a critical role in its superconductivity. A single-phase superconducting compound occurs only in a narrow range of carbon content ($0.85<x<1.0$).[16] Shan *et al.* investigated the specific heat of MgC_xNi_3 and showed a difference between the Sommerfeld parameters of the superconducting (x close to 1) and nonsuperconducting (x about 0.85) samples.[17] They proposed that the disappearance of superconductivity is due to a substantial depression of the electron-phonon coupling caused by decreasing x. Recently, a ^{13}C isotope effect with $\alpha_C=0.54(3)$ was reported, which indicates that $MgCNi_3$ is predominantly a phonon-mediated superconductor and confirms the important role of carbon in superconductivity.[18]

The synthesis of $MgCNi_3$ requires an excess of both Mg and C to compensate for Mg evaporation and to ensure carbon incorporation. Therefore controlled doping of both the Mg site and the C site is difficult, and crystal structure analysis is required to determine the true composition. Previous experiments with hole doping on the Ni site revealed a decrease of T_C. However, to the best of our knowledge, no attempts have been reported on doping the C site in $MgCNi_3$. In this case, considering the covalent radii of the elements, there are two obvious candidates for substitution: boron and nitrogen. Here we report a study of superconductivity in $MgC_{1-x}B_xNi_3$.

II. EXPERIMENTAL SECTION

A series of 0.4 g samples with compositions $Mg_{1.2}C_{1.5-x}{}^{11}B_xNi_3$ ($x=0$, 0.05, 0.1, 0.15, 0.2, and 0.25) was synthesized. The starting materials were bright Mg flakes (99% Aldrich Chemical), fine Ni powder (99.9% Johnson Matthey and Alfa Aesar), glassy carbon spherical powder (Alfa Aesar), and enriched boron metal powder ^{11}B (99.5 at. % ^{11}B—Eagle-Picher Ind., Inc.). The previous studies on $MgCNi_3$ indicated the need to employ excess magnesium and carbon in the synthesis in order to obtain an optimal carbon content.[2,16] The excess Mg is mainly vaporized during the course of the reaction, though MgO is often present in the final product. After thorough mixing, the starting materials were pressed into pellets, wrapped in Zirconium foil, placed on an Al_2O_3 boat, and fired in a quartz-tube furnace under a 95% Ar/5% H_2 atmosphere. The initial furnace treatment began with a $\frac{1}{2}$ h at 600 °C, followed by 1 h at 900 °C. After cooling, the samples were reground, pressed into pellets, and placed back in the furnace under identical conditions at 900 °C. The latter step was repeated three additional times. Following the final heat treatment, the samples were analyzed with powder x-ray diffraction using Cu Kα radiation.

To avoid the problem of neutron absorption of the natural-abundance B, the samples for the neutron-diffraction experiments were prepared with a 95% isotopically enriched ^{11}B. The time-of-flight neutron-powder-diffraction data were collected on the special environment powder diffractometer[19] (SEPD) at the intense pulsed neutron source (IPNS) at Argonne National Laboratory. Diffraction data were collected for samples of nominal composition $MgC_{1.5-x}{}^{11}B_xNi_3$ with $x=0$, 0.05, 0.10, 0.15, 0.20, and 0.25 at room temperature. The high-resolution backscattering data ($2\Theta=144.85°$, bank 1) were analyzed using the Rietveld refinement method with the GSAS (EXPGUI) suite.[20,21] Since the C and ^{11}B neutron-

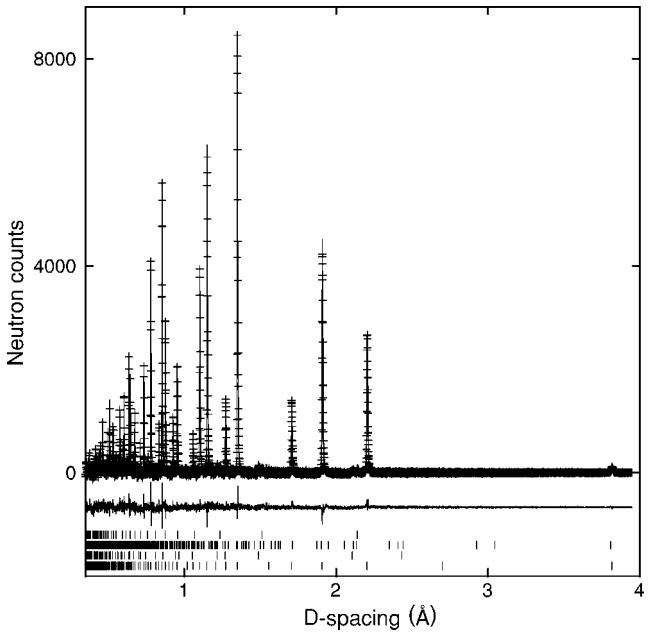

FIG. 1. Rietveld refinement plot showing the observed (+) and calculated (solid line) diffraction data and their difference for $MgC_{1.5-x}{}^{11}B_xNi_3$, $x=0.15$ at room temperature. The tick marks, from the top to the bottom, indicate the intermetallic perovskite phase, MgO, $MgNi_{2.5}B_2$, and vanadium from the sample holder, respectively.

scattering lengths are essentially identical (0.665×10^{-12} cm and 0.666×10^{-12} cm, respectively), only the total occupancy of the (C,B) site in the perovskite $Mg(C_{1-x}B_x)Ni_3$ phase was refined. When $MgNi_{2.5}B_2$ was present, its structural parameters were fixed to those obtained in a previous detailed study,[22] with the phase fraction and cell parameters being the only variables.

III. RESULTS AND DISCUSSION

A typical Rietveld plot is shown in Fig. 1 for the example of the $x=0.15$ sample. All the samples of nominal composition $Mg(C_{1.5-x}B_x)Ni_3$ contain MgO, and in the samples with $x<0.05$, the $MgNi_{2.5}B_2$ phase is also observed (Fig. 2). The MgO fraction is around 2% for the whole doping series, and the $MgNi_{2.5}B_2$ fraction grows very slightly with B concentration up to $x=0.20$, and rapidly increases for $x=0.25$ from about 1.3% ($x=0.2$) to 3.5% ($x=0.25$). At the same concentration, the weight fraction of $MgC_{1-x}{}^{11}B_xNi_3$ drops from 97% ($x=0.2$) to almost 94% ($x=0.25$). This indicates that $x=0.25$ exceeds the boron solubility limit in $MgC_{1-x}{}^{11}B_xNi_3$. This is somewhat greater than the carbon solubility limit (10%) in $Mg(B_{1-x}C_x)_2$.[23]

The C site in this intermetallic perovskite was found to be underoccupied in the whole x range (Fig. 3) in agreement with previous reports.[16,24] To determine the boron-doping level, due to the presence of $MgNi_{2.5}B_2$, it was required to show that carbon does not substitute in the boron position in that phase. Therefore, a series of samples with nominal composition $MgNi_{2.5}B_{2-y}C_y$ ($y=0$, 0.125, 0.25, 0.375, and 0.50) was prepared. The same synthesis procedure was employed. In Fig. 4, the high-angle region of the x-ray diffraction patterns of all samples is presented. The distinct $\alpha_1-\alpha_2$ splitting confirms the high quality of samples. There is no visible shift of the (214), (303), (220), and (206) peaks, indicating that there is no change in the unit-cell parameter. Least-squares

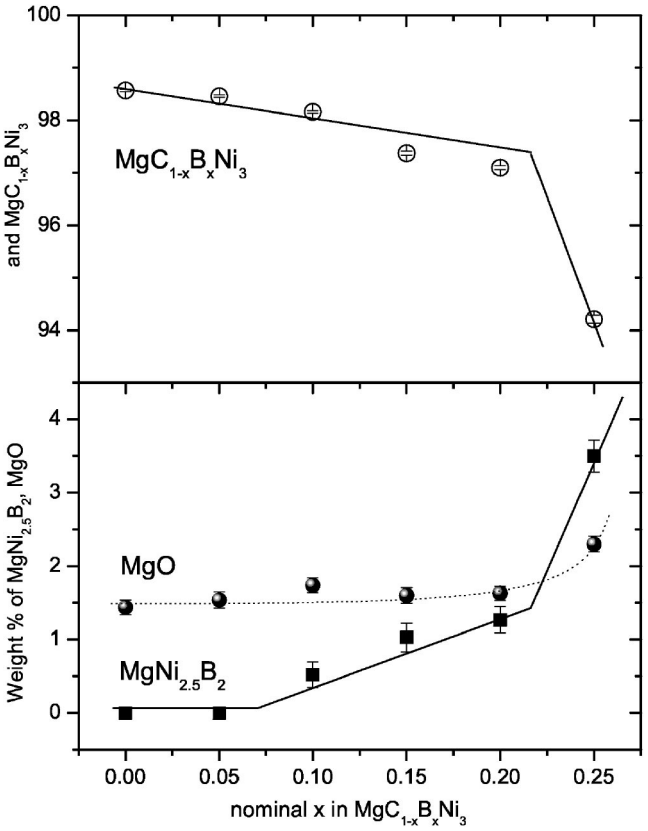

FIG. 2. The refined weight fractions of the intermetallic perovskite phase, MgO, and $MgNi_{2.5}B_2$ as a function of nominal B content.

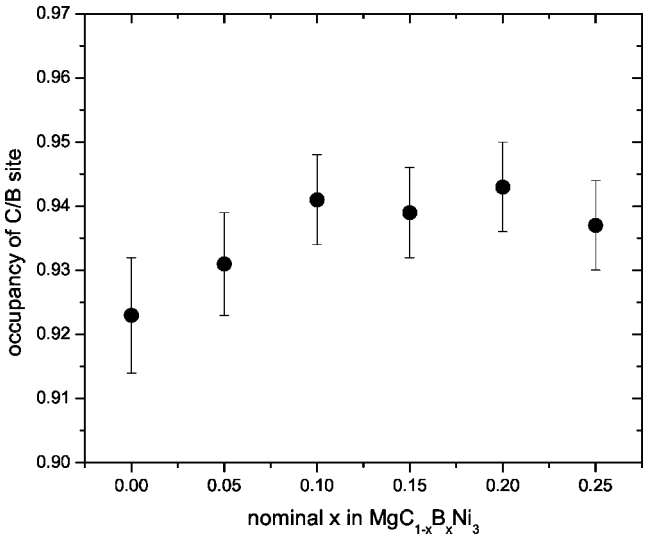

FIG. 3. Total occupancy of the (C/B) site in $Mg(C_{1-x}B_x)Ni_3$ as a function of nominal boron content.

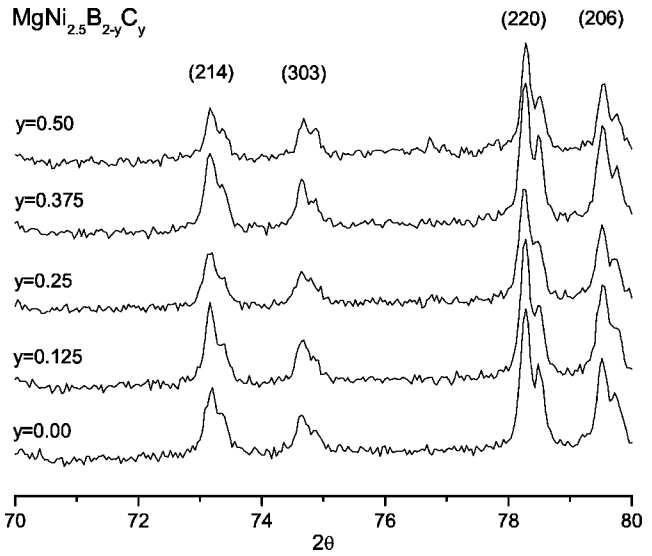

FIG. 4. Powder x-ray diffraction data (CuK_α) for $MgNi_{2.5}B_{2-y}C_y$ for $y=0$, 0.125, 0.25, 0.375, and 0.5.

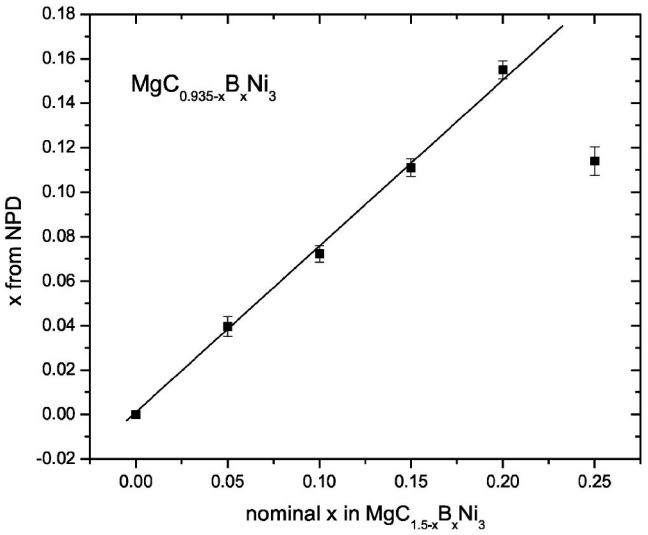

FIG. 5. Boron content in the intermetallic perovskite phase, as determined by neutron diffraction, as a function of nominal boron content.

fits to the 20 strongest x-ray reflections between 20° and 90° 2θ give the unit-cell parameters: $a=4.8801(15)$ Å and 4.8797(11) Å, and $c=8.788(2)$ Å and 8.787(2) Å for nominal $x=0$ and 1.0, respectively. These are consistent with the reported values $a=4.887(2)$ Å, $c=8.789(4)$ Å.[22] This difference in cell parameters is less than 1 part in 10^4, whereas in comparison, the change in the cell parameter for a 15% B substitution for C in $MgCNi_3$ (see below) is 2 parts in 10^3. Given that carbon and boron have different covalent radii, the lack of change to high precision in the cell parameters in $MgNi_{2.5}B_2$ indicates that there is no solubility of carbon in this phase.

The boron distribution between the intermetallic perovskite phase and $MgNi_{2.5}B_2$ can therefore be specified by Eq. (1),

$$MgC_{1-x}B_xNi_3 = MgC_{z-w}B_wNi_3 + (x-w)/2\ MgNi_{2.5}B_2. \quad (1)$$

It is known from the refinement that z has about the same value (~ 0.935) for all samples (Fig. 3), and therefore there is only one unknown, w, in Eq. (1). This value can be found from the experimentally determined weight fractions of the perovskite and $MgNi_{2.5}B_2$ phases.

Figure 5 indicates that the data analysis as described above reveals a linear relationship between the calculated x value and the nominal x in $MgC_{1.5-x}{}^{11}B_xNi_3$ for $x<0.25$. The last point ($x=0.25$) does not follow the trend, confirming that $x=0.25$ exceeds the boron solubility limit of boron in $MgC_{1.5-x}{}^{11}B_xNi_3$. Therefore, the further discussion will consider only samples with nominal $x<0.25$.

The boron concentration dependence of the lattice constant a is shown in Fig. 6. For low B contents ($x<0.04$) the lattice constant changes slightly as the B doping is increased. For greater x, the lattice expands linearly, from $a=3.812\,28(2)$ Å to 3.819 66(2) Å for the lowest ($x=0.0396$) and highest ($x=0.155$) doping levels, respectively. This is consistent with the fact that carbon's covalent radius is smaller than that of boron.

Finally, magnetic measurements were made using a commercial superconducting quantum interference device (SQUID) magnetometer (Quantum Design). The superconducting properties were characterized by zero-field-cooled dc magnetizations ($H_{dc}=10$ Oe) from 2 K to 8 K (magnetic property measurement system—Quantum Design). As seen in Fig. 7, in all cases superconductivity remains bulk in character; however, smaller diamagnetism is visible for doped samples. The last figure (Fig. 8) shows the dependence of the superconducting critical temperature (T_C) as a function of boron doping. T_C was determined as the temperature where the extrapolation of the steepest slope of $\chi_{dc}(T)$ in the superconducting state intersects the extrapolation of the normal

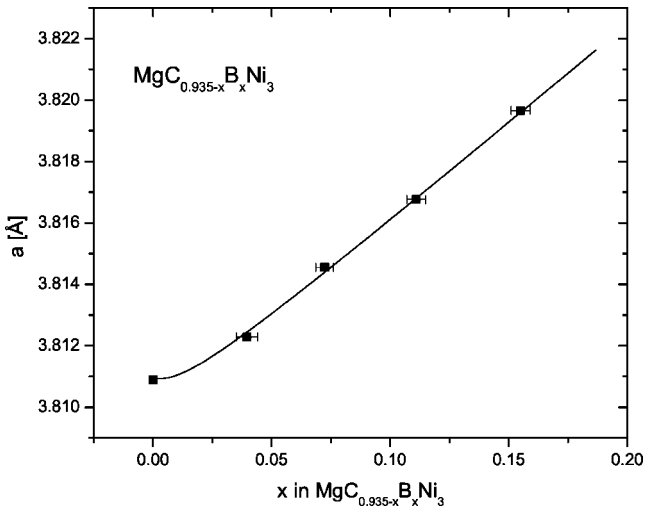

FIG. 6. The cubic-cell parameter as a function of the experimentally determined boron content in the intermetallic perovskite phase. The curve is a guide to the eye.

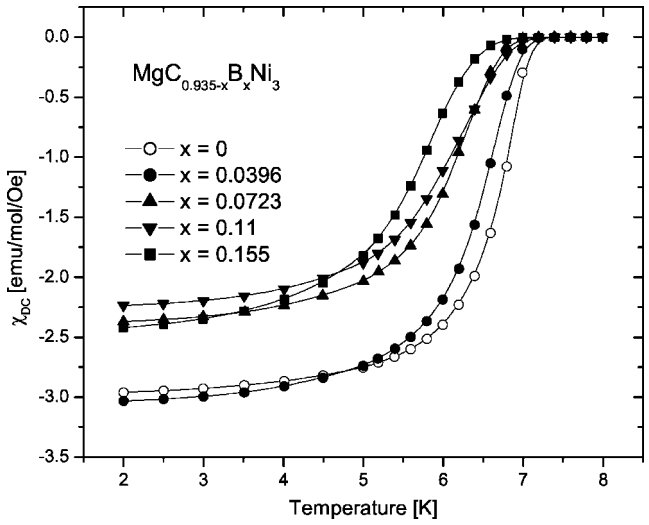

FIG. 7. dc-magnetization characterization of the superconducting transition for all $MgC_{0.935-x}{}^{11}B_xNi_3$ samples, with boron content as determined by neutron diffraction.

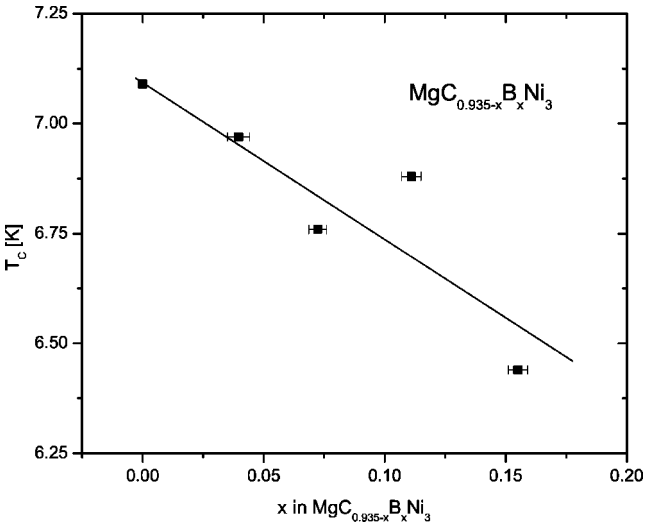

FIG. 8. Superconducting critical temperature (T_C) as a function of x in $MgC_{0.935-x}{}^{11}B_xNi_3$.

state to lower temperatures.[18] The x values are those determined in the neutron-diffraction experiments. As can be clearly seen in Fig. 8, T_c decreases as the boron content decreases: T_C changes from 7.09 K to 6.44 K going from the undoped sample ($x=0$) to the highly doped sample ($x=0.155$). This change in T_c is relatively small compare to that in $Mg(B_{1-x}C_x)_2$, in which 10% carbon doping decreases T_c to 22 K.[23]

In the simplest picture, considering the calculated DOS, hole doping should increase the DOS at E_F and, as a result, T_C should increase. However, this effect is not observed in the case of partial substitutions on the Ni site in $MgCNi_{3-x}M_x$ (M=Co, Fe, Ru, Mn).[11–15] The experiments showed that the DOS peak near E_F decreases in cobalt-doped and carbon-deficient samples.[7,10] More recently, the depression of T_C with increasing carbon deficiency in $MgC_{1-x}Ni_3$ was proposed to be due to a substantial depression of electron-phonon coupling.[17] Either of these effects could account for the lack of T_C enhancement on hole doping, as observed in these cases and also in the case of $MgC_{1-x}B_xNi_3$.

IV. CONCLUSIONS

Our neutron-powder-diffraction studies indicate that the true boron solubility limit in $MgC_{1-x}B_xNi_3$ is 0.16. The magnetic susceptibility measurements show that all samples are superconductors: however, superconductivity is suppressed slowly with increasing x. Although the substitution of boron for carbon is expected to be the least structurally and electronically disruptive of all the chemical substitutions so far successful in $MgCNi_3$, due to the chemical similarity of B and C, this substitution decreases the T_c, suggesting that $MgCNi_3$ has optimal superconducting properties at its intrinsic composition and electron count. The mixing of carbon and boron on the B site in MgB_2 has a substantial effect on $H_{c2}(T)$.[25,26] Analogies between the role of B in that compound and C in $MgCNi_3$ suggest that study of $H_{c2}(T)$ in B substituted $MgCNi_3$ may be of interest.

ACKNOWLEDGMENT

This work was supported by the U.S. Department of Energy, Grant No. DOE-FG02-98-ER45706.

*Present address: Bragg Institute, Australian Nuclear Science and Technology Organization, Lucas Heights, NSW 2234, Australia.

[1] J. Nagamatsu, N. Nakagawa, T. Muranaka, Y. Zenitani, and J. Akimitsu, Nature (London) **410**, 63 (2001).

[2] T. He, Q. Huang, A. P. Ramirez, Y. Wang, K. A. Regan, N. Rogado, M. A. Hayward, M. K. Haas, J. J. Slusky, K. Inumara, H. W. Zandbergen, N. P. Ong, and R. J. Cava, Nature (London) **411**, 54 (2001).

[3] S. B. Dugdale and T. Jarlborg, Phys. Rev. B **64**, 100508(R) (2001).

[4] A. Szajek, J. Phys.: Condens. Matter **13**, L595 (2001).

[5] D. J. Singh and I. I. Mazin, Phys. Rev. B **64**, 140507(R) (2001).

[6] J. H. Shim, S. K. Kwon, and B. I. Min, Phys. Rev. B **64**, 180510(R) (2001).

[7] I. R. Shein, A. L. Ivanovskii, E. Z. Kurmaev, A. Moewes, S. Chiuzbian, L. D. Finkelstein, M. Neumann, Z. A. Ren, and G. C. Che, Phys. Rev. B **66**, 024520 (2002).

[8] J. L. Wang, Y. Xu, Z. Zeng, Q. Q. Zeng, and H. Q. Lin, J. Appl. Phys. **91**(10), 8504 (2002).

[9] H. Rosner, R. Weht, M. D. Johannes, W. E. Pickett, and E. Tosatti, Phys. Rev. Lett. **88**, 027001 (2002).

[10] I. G. Kim, J. I. Lee, and A. J. Freeman, Phys. Rev. B **65**, 064525 (2002).

[11] M. A. Hayward, M. K. Haas, A. P. Ramirez, T. He, K. A. Regan, N. Rogado, K. Inumaru, and R. J. Cava, Solid State Commun. **119**, 491 (2001).

[12] T. G. Kumary, J. Janaki, A. Mani, S. M. Jaya, V. S. Sastry, Y. Hariharan, T. S. Radhakrishnan, and M. C. Valsakumar, Phys. Rev. B **66**, 064510 (2002).
[13] T. Klimczuk, V. Gupta, G. Lawes, A. P. Ramirez, and R. J. Cava, Phys. Rev. B **70**, 094511 (2004).
[14] T. Klimczuk and R. J. Cava, Solid State Commun. **132**, 379 (2004).
[15] A. Das and R. K. Kremer, Phys. Rev. B **68**, 064503 (2003).
[16] T. G. Amos, Q. Huang, J. W. Lynn, T. He, and R. J. Cava, Solid State Commun. **121**, 73 (2002).
[17] L. Shan, K. Xia, Z. Y. Liu, H. H. Wen, Z. A. Ren, G. C. Che, and Z. X. Zhao, Phys. Rev. B **68**, 024523 (2003).
[18] T. Klimczuk and R. J. Cava, Phys. Rev. B **70**, 212514 (2004).
[19] J. D. Jorgensen, J. Faber Jr., J. M. Carpenter, R. K. Crawford, J. R. Haumann, R. L. Hittermann, R. Kleb, G. E. Ostrowski, F. J. Rotella, and T. G. Worlton, J. Appl. Crystallogr. **22**, 321 (1989).
[20] A. C. Larson and R. B. Von Dreele, General Structure Analysis System (GSAS), Los Alamos National Laboratory Report No. LAUR 86-748, 2004 (unpublished).
[21] B. H. Toby, J. Appl. Crystallogr. **34**, 210 (2001).
[22] W. Jung, Z. Naturforsch. B **32**, 1371 (1977).
[23] M. Avdeev, J. D. Jorgensen, R. A. Ribeiro, S. L. Budko, and P. C. Canfield, Physica C **387**, 301 (2003).
[24] Q. Huang, T. He, K. A. Regan, N. Rogado, M. Hayward, M. K. Haas, K. Inumaru, and R. J. Cava, Physica C **363**, 215 (2001).
[25] R. A. Ribeiro, S. L. Bud'ko, C. Petrovic, and P. C. Canfield, Physica C **384**, 227 (2003).
[26] T. Masui, S. Lee, A. Yamamoto, H. Uchiyama, and S. Tajima, Physica C **412–414**, 303 (2004).